Acta Crystallographica Section A
Foundations of Crystallography
ISSN 0108-7673

Received 15 September 2009
Accepted 30 November 2009

Excited-state molecular structures captured by X-ray transient absorption spectroscopy: a decade and beyond

Lin X. Chen,[a,b]* Xiaoyi Zhang,[c] Jenny V. Lockard,[a] Andrew B. Stickrath,[a] Klaus Attenkofer,[c] Guy Jennings[c] and Di-Jia Liu[a]

[a]Chemical Sciences and Engineering Division, Advanced Photon Source, Argonne National Laboratory, 9700 South Cass Avenue, Argonne, IL 60430, USA, [b]Chemistry Department, Northwestern University, 2145 Sheridan Road, Evanston, IL 60208, USA, and [c]X-ray Sciences Division, Advanced Photon Source, Argonne National Laboratory, 9700 South Cass Avenue, Argonne, IL 60430, USA. Correspondence e-mail: lchen@anl.gov

Transient molecular structures along chemical reaction pathways are important for predicting molecular reactivity, understanding reaction mechanisms, as well as controlling reaction pathways. During the past decade, X-ray transient absorption spectroscopy (XTA, or LITR-XAS, laser-initiated X-ray absorption spectroscopy), analogous to the commonly used optical transient absorption spectroscopy, has been developed. XTA uses a laser pulse to trigger a fundamental chemical process, and an X-ray pulse(s) to probe transient structures as a function of the time delay between the pump and probe pulses. Using X-ray pulses with high photon flux from synchrotron sources, transient electronic and molecular structures of metal complexes have been studied in disordered media from homogeneous solutions to heterogeneous solution–solid interfaces. Several examples from the studies at the Advanced Photon Source in Argonne National Laboratory are summarized, including excited-state metalloporphyrins, metal-to-ligand charge transfer (MLCT) states of transition metal complexes, and charge transfer states of metal complexes at the interface with semiconductor nanoparticles. Recent developments of the method are briefly described followed by a future prospective of XTA. It is envisioned that concurrent developments in X-ray free-electron lasers and synchrotron X-ray facilities as well as other table-top laser-driven femtosecond X-ray sources will make many breakthroughs and realise dreams of visualizing molecular movies and snapshots, which ultimately enable chemical reaction pathways to be controlled.

1. Introduction

Chemists have long aspired to visualize molecules in action and control reactions to desirable products. The first step is therefore to find ways of tracking molecules as they change electronic and nuclear configurations and to understand how and why these processes happen. The emergence of two technologies has enabled the first step to become a reality in the past decade. High-intensity pulsed X-rays from third-generation synchrotron sources as well as table-top laser-driven sources have provided the bases for taking snapshots of molecular structures with unprecedented time resolution, *i.e.* 30–100 ps for the past 15 years (http://www.lightsources.org/cms/). Reliable high-intensity ultrafast lasers provide stable sources to excited molecules in a controllable manner. More recently, several X-ray free-electron lasers as the fourth-generation X-ray sources with pulse duration of 50–200 fs are being used and more are being constructed around the world (http://www.lightsources.org/cms/). It is perhaps a good time to reflect on the time-resolved X-ray structural studies in the past decade and to propose or project new frontiers in the future.

As a fast-growing field in the past decade, it is difficult to include a comprehensive list of all the work done in this area even within the same X-ray technique, such as X-ray transient absorption (XTA) spectroscopy (Chen *et al.*, 2001, 2002, 2003*a*,*b*, 2004, 2007; Oulianov *et al.*, 2002; Saes *et al.*, 2003; Chen, 2003, 2004, 2005; Cavalleri *et al.*, 2005; Cannizzo *et al.*, 2006; Khalil *et al.*, 2006; Della-Longa *et al.*, 2009; Gawelda *et al.*, 2007*a*; Shaw *et al.*, 2007*b*; Nozawa *et al.*, 2007; Shan *et al.*, 2007; Smolentsev *et al.*, 2008; van der Veen *et al.*, 2009; Bressler *et al.*, 2009; Lessing *et al.*, 2008). The recent work on photo-induced spin state transitions of Fe(II) complexes has advanced the early work to the femtosecond regime at a synchrotron source (Bressler *et al.*, 2009). Therefore, we will

mainly focus here on our own past and current research of transient molecular structural studies relevant to solar energy conversion and utilization. Meanwhile, as more molecules are being studied by XTA, its advantages and limitations become clearer. Our main goal in this review is to share with others our understanding and experience in this field. A decade of our XTA studies can be divided into three categories as described below. Work in this area is far from complete, as a deeper and better understanding still requires utilization of both synchrotron and the fourth-generation sources for resolving transient structures on different time scales.

2. Structural dynamics of excited-state metalloporphyrins

Metalloporphyrins are analogs of natural pigments, chlorophylls in photosynthesis and heme groups in many enzymes (The Porphyrin Handbook, 1999). Their functions have been extensively investigated for a long time. Their intense absorption in the solar spectrum enables light harvesting, energy and electron transfer in natural photosynthesis (Blankenship, 2002), while their ligation capability enables them to play important roles in catalysis (Collman *et al.*, 1979; Lyon *et al.*, 1991; Nam *et al.*, 2000; Rosenthal & Nocera, 2007). Of course, these functions originate from their unique electronic structures as well as nuclear structures. We chose metalloporphyrin as the first molecules to study by pulsed X-rays because of their relevance to our ongoing research in photosynthesis and their excited-state functions as electron donors to initiate photoinduced electron transfer in many artificial photosynthetic systems. Although studies on their excited-state structure–function correlations have been extensive, most of the structural information has been learned indirectly from optical studies and quantum mechanical calculations before XTA became available.

2.1. Nickel(II) porphyrins

As an example, an excited-state road map of NiTMP [nickel(II)tetramesityl porphyrin] is shown in Fig. 1, based on the work largely by Holten *et al.* on an almost identical molecule NiTPP [nickel(II)tetraphenyl porphyrin] (Kim & Holten, 1983; Kim *et al.*, 1983, 1984; Rodriguez & Holten, 1989, 1990) as well as our own studies on three different Ni(II) porphyrins including NiTMP (Zhang *et al.*, 2007). This example demonstrates several typical photochemical reactions in metalloporphyrins. The ground-state NiTMP has two possible structures depending on the solvent. In non-ligating solvents, such as toluene, it has a square-planar coordination, whereas in ligating solvents, such as pyridine, piperdine and pyrrolidine, it has an octahedral coordination, binding with two axial ligands to Ni(II) (Kim & Holten, 1983; Kim *et al.*, 1983, 1984; Rodriguez & Holten, 1989, 1990). Both forms of NiTMP can be excited through two π–π^* transitions at *Q*- and *B*-bands, with peaks at 530 and 425 nm, respectively. The square-planar NiTMP has a singlet ground state S_0 that can be transformed to the higher singlet excited state *via* the *Q*- or *B*-band excitation, and the dual ligated octahedral NiTMP has a triplet ground state T_0 that can be excited to the higher triplet states *via* the the *Q*- or *B*-band excitation at slightly different energies (Chen *et al.*, 2001; Kim *et al.*, 1983; Rodriguez &

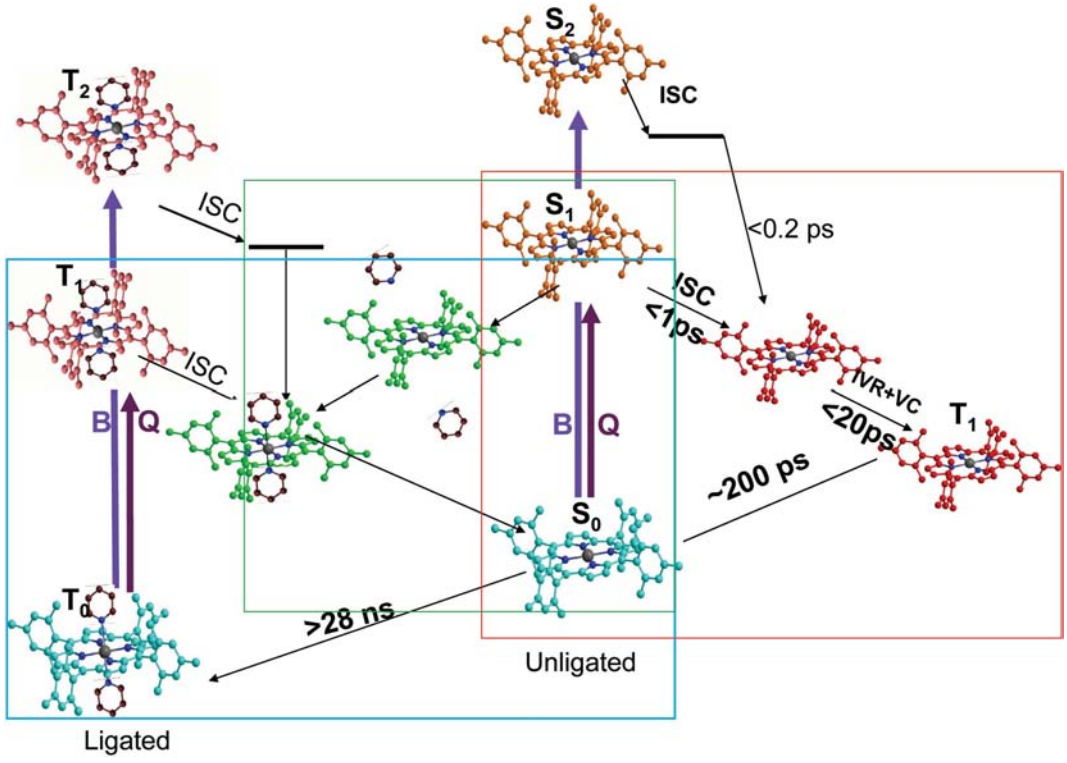

Figure 1
The excited-state pathways of Ni(II)TMP or NiTPP in solution. ISC: intersystem crossing; IVR: internal vibrational relaxation; VC: vibrational cooling.

Holten, 1990). The transformations from one state to another take place with time constants ranging from less than 200 fs to tens of nanoseconds (Fig. 1).

The color-coded boxes in Fig. 1 highlight three individual processes studied using XTA as well as optical transient absorption spectroscopy (Chen *et al.*, 2007, 2001, 2010). The first known solution pump–probe XTA spectrum leading to structural determination using the pulsed nature of the X-rays from a synchrotron source was performed in 1999–2000 (Chen *et al.*, 2001) at the APS in Argonne National Laboratory for the process outlined in the blue box, except the molecule studied then was NiTPP. A cluster of six X-ray pulses was used to probe a recombination process of two axial piperdine ligands with NiTPP after they were photodissociated by a laser pulse at 351 nm. The process has a time constant of 28 ns, which is sufficiently long for the 14 ns time window of the X-ray pulse cluster to capture the intermediate. The results demonstrated that (i) XTA measurements at a synchrotron source are feasible with a dilute solution of 1 m*M* for NiTPP, (ii) singlet X-ray probe pulses with similar X-ray photon flux per pulse can be used to achieve 100 ps time resolution limited only by the X-ray pulse duration, (iii) there are advantages and disadvantages of using the then available solid-state Ge detector array, and (iv) the photodissociation intermediate is square-planar under the time resolution limit. The top process of the blue box, the photodissociation, remains to be explored in our future experiments.

The process outlined in the red box was the next set of excited-state structural dynamics to be explored by the XTA method. The electronic configuration of Ni(II) ($3d^8$) in an almost square-planar ground state S_0 has an empty $3d_{x2\text{-}y2}$ molecular orbital (MO) and a doubly occupied $3d_{z2}$ MO (Ballhausen, 1962). The $S_0 \rightarrow S_1$ transition in NiTMP can be induced by exciting the *Q*-band with 527 nm light. Within 350 fs following the excitation, the S_1 state was believed to convert, through energy transfer, to an intermediate state T_1' that then undergoes vibrational relaxation to a relaxed triplet state, T_1, with a presumed $^3(3d_{x2\text{-}y2}, 3d_{z2})$ configuration, where $3d_{x2\text{-}y2}$ and $3d_{z2}$ MOs are each singly occupied (Kim *et al.*, 1983; Rodriguez & Holten, 1989; Gentemann *et al.*, 1997; Eom *et al.*, 1997). The T_1 state returns to the S_0 state in approximately 200 ps. The electronic configurations of these excited states have been assigned largely according to computational results. Before we interrogated the electronic configuration and the geometry of the T_1 state using XTA measurements, the geometric structures of these excited states were still subject to many uncertainties (Chen *et al.*, 2007).

In the XANES region, especially the pre-edge region, a single peak due to the $1s \rightarrow 3d_{x2\text{-}y2}$ transition in the S_0 state and two peaks due to the $1s \rightarrow 3d_{x2\text{-}y2}$ and $1s \rightarrow 3d_{z2}$ transitions in the T_1 state have been experimentally observed, confirming that the excited T_1 state has two singly occupied $3d_{x2\text{-}y2}$ and $3d_{z2}$ MOs (Fig. 2*a*). This result was obtainable heretofore only *via* theoretical calculations. Therefore, XTA inferred excited-state MO energy levels through X-ray-induced electronic transitions from the core to valence levels while the molecules are optically excited. In particular, this method is complementary to optical transient absorption spectroscopy but has advantages for correlating molecular geometry with electronic configurations and MO energy levels when the excited state is optically 'dark' or overwhelmed by other strongly absorbing or emitting states. The other striking observation at the pre-edge region is the difference in the bandwidth for the $1s \rightarrow 3d_{x2\text{-}y2}$ and $1s \rightarrow 3d_{z2}$ transitions in NiTMP. The implication of the bandwidth difference is related to the structural dynamics observed in previous Raman spectroscopic studies (Schweitzer-Stenner *et al.*, 2001; Lemke *et al.*, 1998; Jia *et al.*, 1998), and will be addressed in detail in our future publication (Chen *et al.*, 2010).

As the excited NiTMP proceeds through an energy cascade along the path $S_1 \rightarrow T_1$, the excess energy from the (π, π^*) state generates vibrationally hot states causing molecular geometry rearrangements. Consequently, average Ni—N and Ni—C_α distances in the T_1 state are lengthened by 0.08 and 0.07 Å, respectively (without phase corrections, Fig. 2*b*), suggesting a porphyrin ring expansion. It is conceivable that

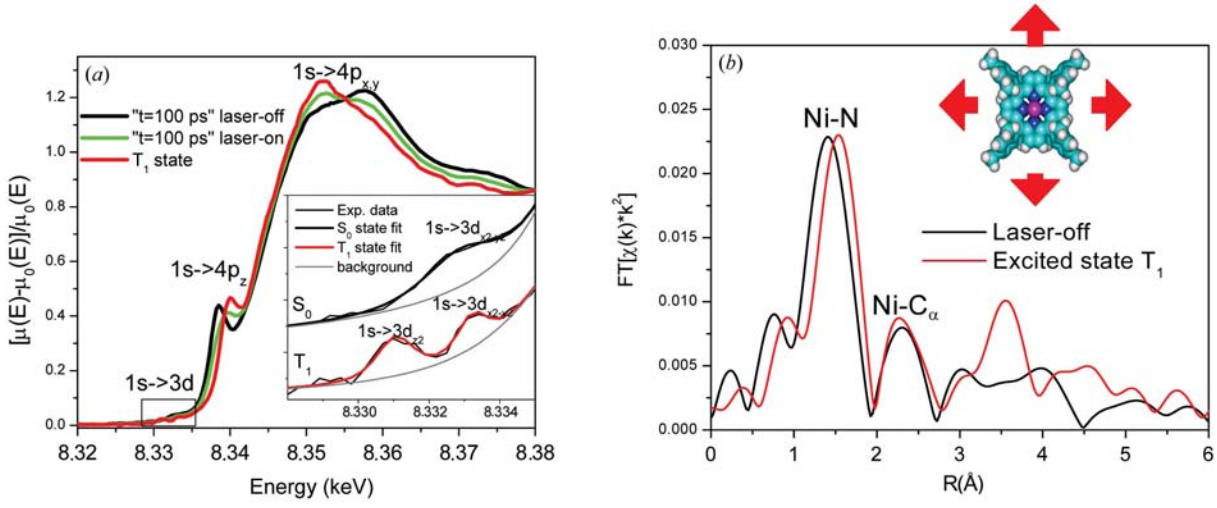

Figure 2
(*a*) XANES spectra of NiTMP; inset: pre-edge region. (*b*) FT-XAFS spectra of NiTMP (Chen *et al.*, 2007).

the addition of one electron to the higher-energy antibonding $3d_{x2\text{-}y2}$ MO in the T_1 state could reduce the bond order for Ni—N bonds, resulting in longer Ni—N bond distances.

In the rising edge region from 8.337 to 8.343 keV, the XANES spectra (Fig. 2*a*) exhibit a distinctive feature assigned as a dipole-allowed $1s \rightarrow 4p_z$ transition (Kau *et al.*, 1987), which is shifted to 1.5 eV higher in energy in the T_1 state than in the S_0 state. This XANES feature is very sensitive to the ligation state of the metalloporphyrin (Chen *et al.*, 2001), which enables us to monitor the photoinduced ligation processes outlined in the green box where the reaction coordinates of NiTMP excited state are investigated during a photo-induced ligation process with pyridine ligands. When the dual axial ligation takes place at either the S_0 or T_1 state, the $1s \rightarrow 4p_z$ transition energy becomes higher which shifts the sharp feature observed in the square-planar NiTMP away to a higher energy overlaid with the white-line peak. Thus, the dual axial ligated NiTMP has a smooth rising edge without the sharp $1s \rightarrow 4p_z$ transition peak. A NiTMP solution in a mixed solvent of toluene and pyridine was photoexcited by 527 nm light where only unligated NiTMP was excited. The XANES spectrum of doubly ligated NiTPP-(piperdine)$_2$ was used as a reference for an octahedral coordination geometry with no distinct $1s \rightarrow 4p_z$ transition feature. If the dual ligation takes place, we expect to see a decrease in the intensity of the $1s \rightarrow 4p_z$ transition feature.

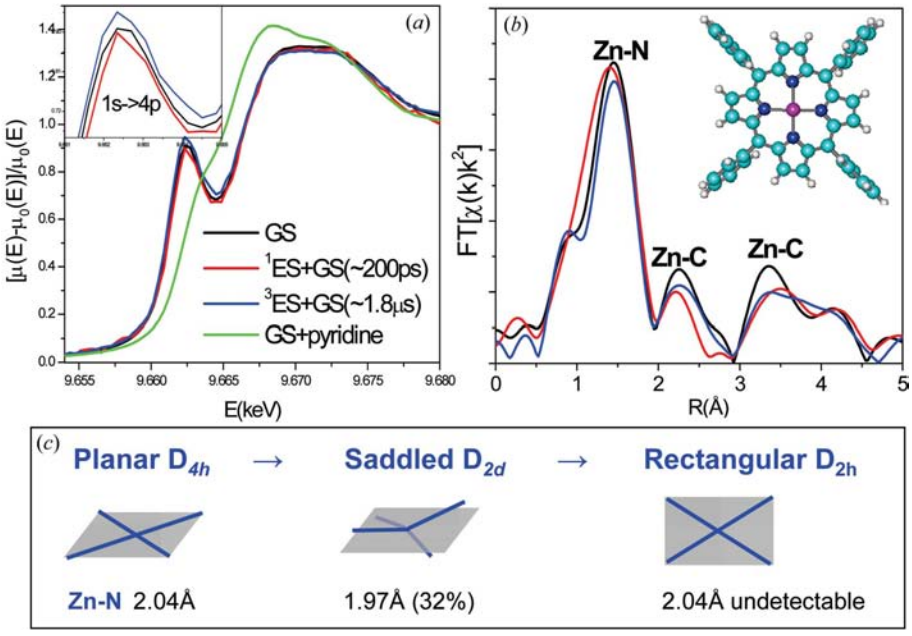

Figure 3
XANES (*a*) and EXAFS (*b*) spectra of the ZnTPP excited state along with those of its ground state and penta-coordinated ZnTPP-pyridine adduct. (*c*) Structural changes of ZnTPP in the singlet and triplet excited states inferred by the XTA measurements.

This expected $1s \rightarrow 4p_z$ transition peak attenuation was not immediately observed until 600 ps after the photoexcitation owing to the formation of NiTMP*-py$_2$. Once the ligated species forms, the time constant for them to return to the ground state is >40 ns, while the excited state of the unligated species lifetime constant is ~200 ps in toluene. Because the ground-state dual ligated NiTMP or NiTPP is a triplet state, the S_1 state must undergo an intersystem crossing to a triplet state before the ligation takes place. Using concentrations of various species measured through both UV–Vis spectroscopy and XTA, the excited-state ligation equilibrium constant for NiTMP* + 2py ↔ NiTMP(py)$_2$* is ~0.07 M^{-2}, a factor of two enhancement compared with that for the ground state. The correlations between the structural diversity and the excited-state properties resulting from this study are important for the elucidation and control of photocatalytic reactions such as fuel generation by sunlight in particular.

2.2. Structural dynamics of other metalloporphyrins

We have also studied other metalloporphyrin excited-state structures, such as ZnTPP (Chen *et al.*, 2006) and CuOEP-(octaethylporphyrin) (Chen *et al.*, 2004) *etc*. As a closed-shell metal center Zn(II) ($3d^{10}$) in ZnTPP does not participate in charge transfer processes, and the structural changes are primarily due to the electron density change in four coordinating N atoms, which are preferentially involved in ZnTPP in HOMO to LUMO transitions. In contrast, ZnOEP has its HOMO to LUMO transition involving mostly more distant C atoms, and hence the excited-state structural changes are smaller than those in ZnTPP. So far, we have only detected a Zn—N bond length decrease from 2.04 Å in the ground state to 1.97 Å in the single excited state of ZnTPP, suggesting a symmetry change from D_{4h} to D_{2d} (Fig. 3) (Chen *et al.*, 2006). Although there was evidence of triplet state structural changes from that of the ground state (Van der Poel *et al.*, 1982), we did not detect the change with XTA for various reasons, which will be reinvestigated again in the future.

Another metalloporphyrin studied is Cu(II)OEP in toluene and in toluene/thf mixture (Chen *et al.*, 2004). The photo-excitation of a Cu(II) porphyrin from $S_0 \rightarrow S_n$ is followed by rapid (*i.e.* <1 ps) intersystem crossing to the excited $^2T_1$ state which equilibrates with another excited state $^4T_1$ (Cunningham *et al.*, 1997; Kim *et al.*, 1984; Kruglik *et al.*, 1995; Liu *et al.*, 1995; McMillin *et al.*, 1993, 1994; Oertling *et al.*, 1987; Shvedko *et al.*, 1999). In addition to the normal π–π^* transitions, two intramolecular charge transfer (CT) transitions between π orbitals of the macrocycle and d orbitals of the metal, d–π^* and π–d transitions, also known as the metal-to-ligand charge transfer (MLCT) and ligand-to-metal charge transfer (LMCT), may take place. Quantum mechanical calculations on Cu-porphyrin suggest that binding a water molecule as an axial ligand lowers the energy of the $^2(3d_{z2}, 3d_{x2\text{-}y2})$ state which favors a five-coordinate complex with a domed structure (Kim *et al.*, 1984; Shelnutt *et al.*, 1984). By

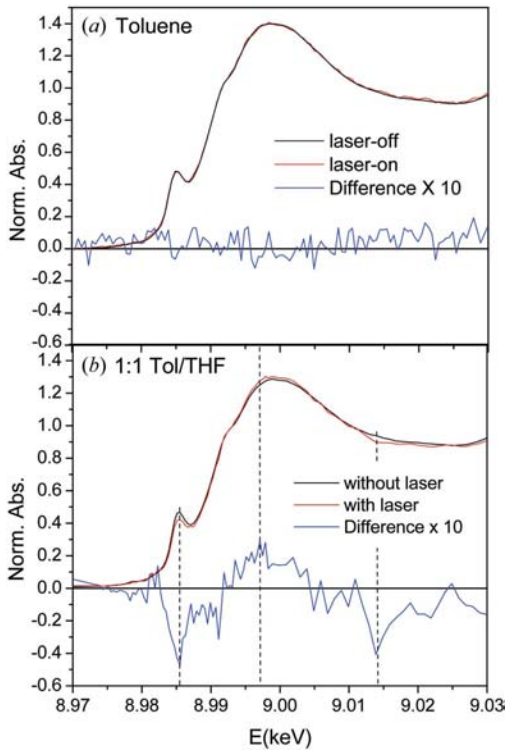

Figure 4
XANES spectra and difference spectra of CuOEP with laser-on and laser-off at a delay time of about 200 ps in (*a*) neat toluene and (*b*) toluene/thf mixture. The attenuation of the $1s \rightarrow 4p_z$ feature shows evidence of the axial ligation in the excited state.

investigating the intensity variation of the XANES feature due to the $1s \rightarrow 4p_z$ transition (Smith *et al.*, 1985), the coordinating status of the Cu in both the ground and excited triplet states can be obtained. XTA enabled unambiguous identification of the axial ligation of Cu in CuOEP triplet state with a 500 ps lifetime in toluene with the presence of oxygen-containing thf as a ligand, forming the 'exciplex' (Fig. 4).

3. MLCT excited-state dynamics of transition metal complexes

The MLCT excited states of many transition metal complexes can be generated by photons in the solar spectrum, resulting in electron density shift from the metal center to its ligands, or $d \rightarrow \pi^*$ transitions (Kalyanasundaram, 1992). If such a charge separation is sustained for a sufficiently long period, it can drive photochemical reactions. Hence, the MLCT transitions are important in applications of luminescent probes (Lu *et al.*, 2004; Lamansky *et al.*, 2001), molecular machines (Collin *et al.*, 2001), dye-sensitized solar cells (Gratzel, 2001), photocatalysis (Esswein & Nocera, 2007) *etc*. In spite of their importance, however, identification of absolute molecular structures of the MLCT excited states have remained elusive until about seven years ago when two groups in Argonne National Laboratory and in University of Lausanne independently and almost simultaneously studied the MLCT excited-state structures of transition metal complexes using XTA (Chen *et al.*, 2002, 2003*a*; Saes *et al.*, 2003). Since then, there have been several other structural dynamics studies on these MLCT states in different transition metal complexes. The MLCT excited states are likely precursors responsible for photochemical reactions, such as water splitting for light-to-fuel conversion (Esswein & Nocera, 2007). Owing to the MLCT transitions, the metal center oxidation states will change, accompanied by changes in coordination geometry and bond distance, all of which can be probed by XTA.

3.1. Cu(I) diimide

We chose to investigate the MLCT state structure of $Cu^{I}(dmp)_2^+$, where dmp is 2,9-dimethyl-1,10-phenanthroline, using the XTA method since there had been the compelling evidence described in literature (McMillin *et al.*, 1985; McMillin & McNett, 1998; Scaltrito *et al.*, 2000*b*; Ruthkosky *et al.*, 1997; Castellano & Meyer, 1997; Miller *et al.*, 1999) for novel structural reorganization following light absorption (Fig. 5). The origin of the photo-driven structural change takes place through the process $Cu^{I}(3d^{10})(dmp)_2^+ + h\nu \rightarrow Cu^{II}(3d^9)(dmp^-)(dmp)^{+*}$, where an electron from Cu(I) is shifted to a ligand. If the ligand is connected to an acceptor for electron or energy, charge separation or Förster energy transfer could occur (Scaltrito *et al.*, 2000*a*; Ruthkosky *et al.*, 1997; Castellano & Meyer, 1997). More interestingly, $Cu^{I}(dmp)_2^+$ derivatives have been used as core functional moieties in molecular machines driven by redox reactions initiated electrochemically or photochemically interconverting Cu(I) and Cu(II) (Sauvage, 2001, 1998; Collin *et al.*, 2001). The coordinating geometry preference of the Cu center at different oxidation states, tetrahedral geometry for Cu(I) and penta- or octahedral geometry for Cu(II), enables the rotational and translational motions in the supermolecule with both moving and stationary parts (Sauvage, 2001, 1998; Collin *et al.*, 2001).

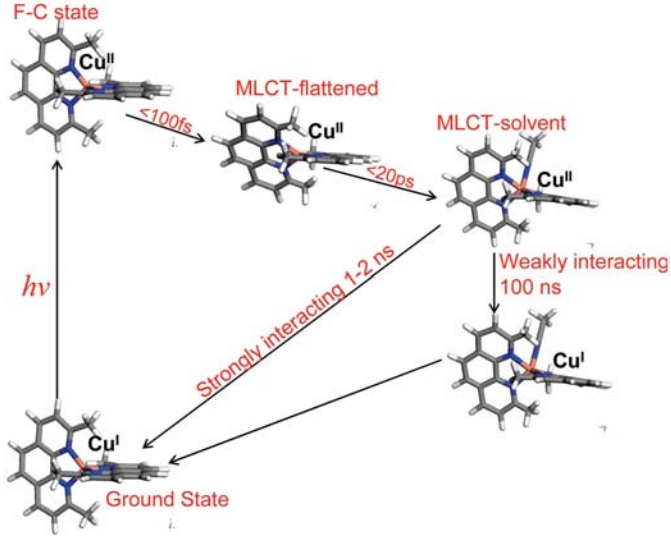

Figure 5
Excited-state reaction pathway and time constants of $[Cu(dmp)_2]^+$ in strongly and weakly coordinating solvents. XTA identified that the exciplex forms in both solvents.

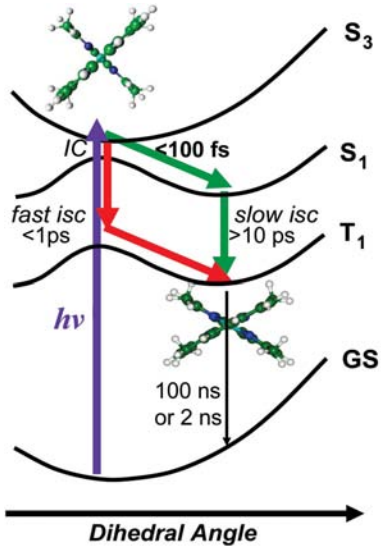

Figure 6
Ultrafast excited-state potential surfaces and reaction pathways of $[Cu(dmp)_2]^+$ based on Siddique *et al.* (2003). Multiple dynamics processes have ligand dihedral angle-dependent rate constants. The fluorescence upconversion (Shaw *et al.*, 2007*a*) revealed a 77 fs prompt fluorescence lifetime assuming from the F–C state, and a >10 ps fluorescence lifetime at the red emission wavelength, assuming from the flattened MLCT state that has the reduced spin–orbital coupling. The flattening time constant of ~100 fs is currently inferred only by optical spectroscopy, while this value can be explored in the future with X-rays on the femtosecond time scale.

The ground-state Cu^I center has a pseudo-tetrahedral coordination geometry (Hamalainen *et al.*, 1979) which can be excited to generate a Franck–Condon (F–C) state with a Cu^{II}* center which is susceptible to the Jahn–Teller distortion to a flattened tetrahedral geometry in the thermally equilibrated MLCT state (Fig. 5) (McMillin & McNett, 1998). Ultrafast optical transient absorption spectroscopy and the fluorescence upconversion results on the MLCT state dynamics of $[Cu^I(dmp)_2]^+$ (Lind *et al.*, 2008; Iwamura *et al.*, 2007; Shaw *et al.*, 2007*b*) revealed a possible ultrafast flattening of the F–C state in <100 fs as well as the geometry-dependent singlet MLCT state lifetime as suggested by Siddique *et al.* using calculated potential surfaces for the ground and excited states as functions of the dihedral angle between the two dmp ligand planes (Fig. 6) (Siddique *et al.*, 2003). A tri-exponential function was used to fit the excited-state dynamics with two solvent-independent time constants of <0.5 ps, 15 ps, and one solvent-dependent time constant of 2 ns in acetonitrile (coordinating solvent), and 100 ns in toluene (non-coordinating solvent) (Chen *et al.*, 2002, 2003*b*; Chen, 2001). The first two time constants suggested the flattening and intersystem crossing time scales, respectively. These steps are too fast to follow with 100 ps synchrotron X-ray pulses. Therefore, only the longest processes for the decay of the thermally equilibrated MLCT state can be monitored by the synchrotron X-ray pulses as in our previous studies (Chen *et al.*, 2002, 2003*b*; Chen, 2001).

Thermally equilibrated MLCT state structures emerging ~20 ps after the excitation were studied by XTA in coordinating acetonitrile and in non-coordinating toluene with the laser excitation at 527 nm. The resulting MLCT spectra in both solvents resemble the ground state of $[Cu^{II}(dmp)_2]^{2+}$ (Fig. 7*a*). FT-EXAFS spectra (Fig. 7*b*) show increased intensities of the Cu—N peak for the laser-excited $[Cu^I(dmp)_2]^+$ in both solvents, suggesting additional ligand binding to $Cu^{(II)}$* in the transient MLCT state. Interestingly, the average Cu—N distance compared with the ground state shifts to a shorter distance in acetonitrile but to a longer distance in toluene. The results of the experiment demonstrated (i) light excitation of $[Cu^I(dmp)_2]^+$ generated a formal Cu^{II}* center in the excited MLCT state, (ii) the inner-sphere reorganization changed the coordination number of the MLCT state from four to five in presumed non-coordinating toluene, and (iii) the average Cu–ligand bond distances lengthened in the MLCT state in toluene, but shortened in acetonitrile. According to the energy gap law (Freed & Jortner, 1970; Bixon *et al.*, 1994; Scaltrito *et al.*, 2000*b*), the non-radiative rate constant increases exponentially with decreasing energy separation between the ground state and the excited state. Although the XTA results in both solvents support the formation of a penta-coordinated Cu^{II}* center in the MLCT state, the respective elongation and shortening of the average Cu—N bond distance for the MLCT state of the $[Cu^I(dmp)_2]^+$ signal the difference in interactions of the Cu^{II}* with the fifth ligand. Toluene has less electron-donating capability compared with acetonitrile, hence it could only act as the fifth ligand with a longer and less stable bond with the Cu^{II}*. Consequently, the MLCT state of the $[Cu^I(dmp)_2]^+$–toluene complex will not be as stable and will not lower the energy of the MLCT state as much as the acetonitrile complex. Hence, the excited-state quenching is only significant in acetonitrile, and the 'exciplex' previously inferred is more appropriate for cases where strong excited-state adducts completely quenched the excited state. In this work we have resolved internal atomic reorganization linked to electron transfer for a MLCT complex, and established a foundation for the proposed future studies of internal reorganization for energy conversion in tuned photoinduced

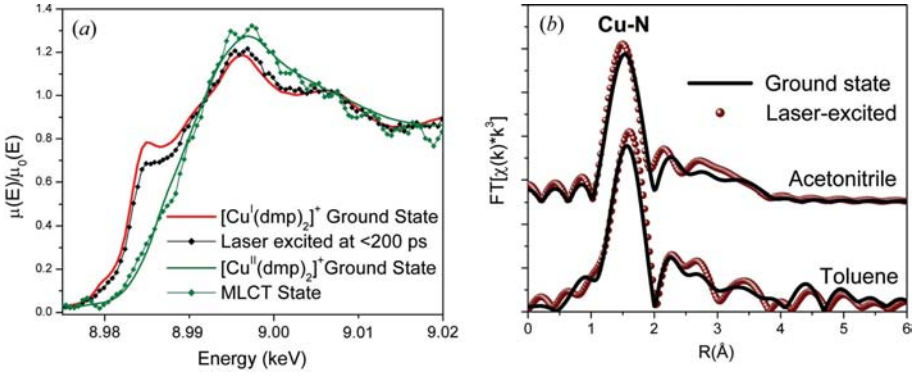

Figure 7
XTA spectra of $[Cu(dmp)_2]^+$ in (*a*) XANES spectra and (*b*) FT-XAFS spectra.

electron transfer complexes. This knowledge can be used in molecular design to investigate the potential replacement of precious metal complexes for dye-sensitized solar cell and photocatalysts with cheaper first-row transition metal complexes (Armaroli, 2008, 2001; Smeigh & McCusker, 2006).

3.2. MLCT states of the second- and third-row transition metal complexes

Many photoactive metal complexes contain later transition metal centers. Accordingly, determining their excited-state structures requires XTA measurements at the *K*- or *L*-edge for the second-row transition metals or the L_{III}-edge of the third-row transition metals. Generally speaking, XANES features of these heavier metals are less distinct than those of the first-row transition metals primarily due to the lifetime broadening. Consequently, high data quality for XTA spectra of these metal centers is necessary for extracting accurate excited-state structural information. The data quality of the current experimental set-up is far superior to that obtained during the early days of our studies, which often missed structural changes that are only obviously visible in the difference spectra (laser-on–laser-off). More recently, we studied MLCT excited-state structures of a platinum dimer complex and a tungsten complex, which will appear in our future publications (Lockard *et al.*, 2010; Lovaasen *et al.*, 2010). We have learned from these studies that the best way to distinguish the structural changes is from analyzing the difference spectra, which has been explored by different groups using different approaches focusing in the XANES region, such as *MXAN* (Benfatto & Della Longa, 2001; Gawelda *et al.*, 2007*b*; Benfatto *et al.*, 2006) and *FitIt* (Smolentsev & Soldatov, 2007, 2006). Using the W-complex as an example, the raw laser-on and laser-off spectra look almost identical. Before recent beamline improvements, one would have mistakenly interpreted these results as no structural difference. However, the difference spectrum with and without the laser pump pulse clearly displays oscillatory features that support the evidence for the bond lengthening in the excited state (Lovaasen *et al.*, 2010). The tungsten–alkylidyne (or carbyne) with formal d^2 octahedral structure can bind ligands with diverse electronic structures, including strong π acids and π donors and hard and soft σ bases (Bocarsly *et al.*, 1985, 1987; Carter *et al.*, 1991; Pollagi *et al.*, 1994; Trammell *et al.*, 1995; Schoch *et al.*, 1996; Xue *et al.*, 1996, 1997, 1998; Lee *et al.*, 1998; Cavalheiro *et al.*, 1999; Mayr *et al.*, 1999; Lai *et al.*, 2001; Simpson *et al.*, 2003; Jelliss & Wampler, 2005), which tunes the photophysical and photoredox properties or even changes the orbital character of the emissive state among $d \rightarrow \pi^*$, $\pi \rightarrow d$ and MLCT manifolds. The structural and electronic diversity of these complexes poses a challenge for interpreting their photophysical properties, such as the nature and the molecular structure of the emissive excited state, through XTA measurements of W(CPh)(dppe)$_2$Cl [dppe = 1,2-bis(diphenylphosphino)ethane] (Fig. 8). Owing to the manuscripts in preparation, only a brief description of our observation can be made here. The difference XTA spectrum in the XANES region clearly shows an electron vacancy created by a photoinduced MLCT transition. Meanwhile, the Fourier-transformed EXAFS spectrum between the laser-off and laser-on spectrum reveals the changes in the local coordination environment around the tungsten metal. The W—C bond length appears to increase upon population of the ^{3}MLCT excited state. The changes in W—P and W—Cl are more difficult to resolve. We are currently working on quantifying these changes by fitting the excited-state XAS spectrum (Lovaasen *et al.*, 2010).

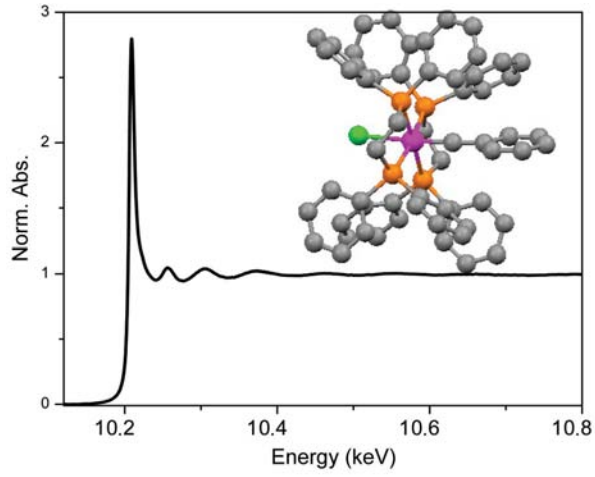

Figure 8
Molecular structure and XAFS spectrum of W(CPh)(dppe)$_2$Cl in toluene. The excited-state spectrum and difference spectrum will appear in the future (Lovaasen *et al.*, 2010).

4. Photogenerated transient species in interfacial heterogeneous systems

Many chemical processes are enabled at the interface where energy, electron and matter transfer take place, driven by energy and electric or chemical potential gradients defined by structures of interfaces. Our understanding of transient structures at the interface will ultimately allow us to design new interfacial materials and apply new driving forces to control chemical reactions.

For interfacial structures on flat surfaces, surface-specific X-ray structural methods (such as grazing-angle X-ray scattering and X-ray absorption) can be coupled with an ultrafast perturbation by light, heat, pressure or electric field to map out reaction coordinates at far from equilibrium conditions during energy and charge flow. The main challenge here is the sample damage by both X-ray and laser afforded by stationary film samples. For interfacial structures at particle surfaces, one can make particle suspensions with the same circulation system as for liquid samples, which is an approach that we have been taking.

4.1. Transient structures of dye sensitizers in solar cell

We have investigated the transient structures of a transition metal complex used in the dye-sensitized solar cell (DSSC)

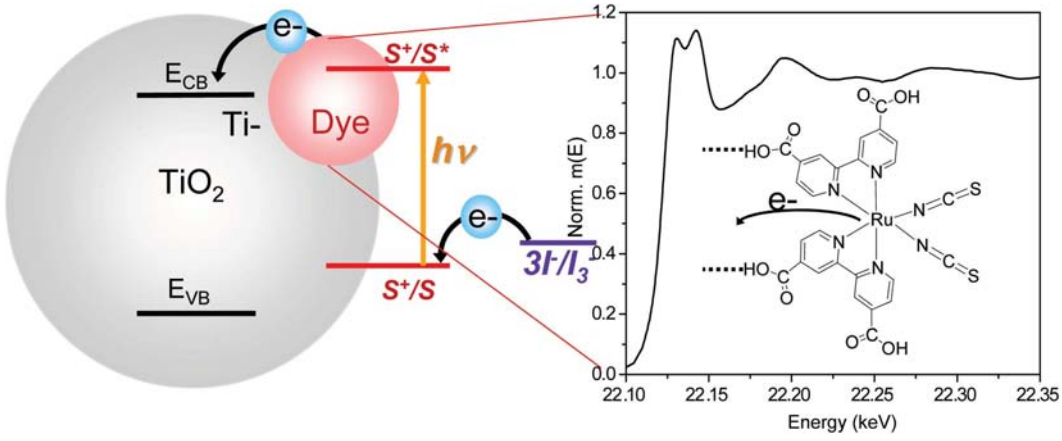

Figure 9
The DSSC mechanism and the XANES spectrum of RuN3 bound on TiO_2 nanoparticle surface. The charge separate state spectrum and difference spectrum will appear in the future (Zhang *et al.*, 2010).

(Bach *et al.*, 1998; Gratzel, 2001; Benko *et al.*, 2004) where dye molecules, such as RnN3 (Fig. 9), with strong absorbance in the solar spectrum are linked to a titanium dioxide (TiO_2) nanoparticle surface as part of an electrode. An optical photon promotes an electron to the MLCT state of the dye, from which an electron is injected into the conduction band of TiO_2. The hole left behind in the dye molecule will be replenished by a redox shuttle of $3I^-/I_3$. It has been shown from quantum mechanical calculations and ultrafast transient optical spectroscopy that the time for the MLCT state of the dye to inject an electron to TiO_2 is less than 100 fs (Cherepy *et al.*, 1997; Gratzel, 2001). The structural consequences of the injection on both TiO_2 surface and the metal complexes as well as prospective control of the injection rate constant from dye to nanoparticles interfacial structure are unknown. Understanding these issues will have significant impact on optimizing the device efficiency and lowering costs, leading to the replacement of Ru complexes with cheaper metal complexes.

The XANES spectrum of RuN3 dye on the TiO_2 nanoparticle surface at the Ru *K*-edge is shown in Fig. 9. The photochemical processes can be expressed as Ru(II)N3 + $(TiO_2)_n$ + $h\nu \rightarrow$ Ru(III)N3 + Ti(III)$O_2(TiO_2)_{n-1}$, where the Ru(II) is oxidized to Ru(III) while one of the Ti(IV) centers is reduced to Ti(III) (Anderson & Lian, 2005). This charge separation will last for microseconds or longer until the Ru(III) can be reduced again by the redox shuttle $3I^-/I_3$ or other reducing reagent. The RuN3 dye on the TiO_2 nanoparticle sample was in a suspension and was circulated during the experiment. The observed Ru *K*-edge for the excited RuN3 dye at 50 ps, long after the injection, is shifted to a higher energy as expected. The data analysis suggests that nuclear arrangements of the dye also take place accompanying the injection. The complete data analysis combined with theoretical calculations is in progress on extracting the edge shift at different times after the injection, as well as nuclear geometry change resulting from this injection process (Zhang *et al.*, 2010).

4.2. Transient states of metal particle catalysts on semiconductor nanoparticle surfaces

The other important and commonly encountered interfacial systems are metal catalyst crystallites coated semiconductor nanoparticles, such as TiO_2, for hydrogen production (Fujishima & Honda, 1972). In this case, semiconductor nanoparticles are light-harvesting antenna. In one of such systems, platinum crystallites on the TiO_2 nanoparticle surface act as a cathode to promote the combination of the electrons and protons in forming hydrogen. Because the proton reduction is more facile on the surface of Pt than TiO_2, hydrogen production is more competitive to the electron–hole recombination. Thus the presence of Pt significantly improves the efficiency of photocatalytic splitting of water.

We studied the Pt oxidation state in Pt/TiO_2 catalysts for hydrogen production using XTA at the Pt L_{III}-edge. Highly dispersed Pt supported by TiO_2 nanoparticles (1 wt% Pt) was prepared. The catalyst powder thus produced was subsequently mixed with water and ball-milled to ensure maximum suspension and minimum catalyst particle size in liquid before the pump–probe experiment. The recycling water/methanol slurry jet with suspended $PtO/Pt/TiO_2$ was used in the XTA study. Laser pulses with 5 ps FWHM at 351 nm were used as the excitation source, promoting charge separation across the band gap of TiO_2 nanoparticles. Only XANES spectra were collected at the L_{III}-edge of Pt at time delays between the pump laser and the probe X-ray pulses, at 0, 1 and 50 round trips of the X-ray pulses in the storage ring where one round trip equals 3.7 µs (Fig. 10). The variation of the Pt white-line peak under different delays clearly demonstrated an oxidation state change of Pt.

We have observed, from the results of this first attempt on such measurements, that (*a*) the starting Pt/TiO_2 catalyst contained both Pt(II) and Pt(0), (*b*) the photoexcitation of TiO_2 apparently causes a small amount of reduction of Pt(II) within 100 ps, indicative of electron transfer and/or by hydrogen formed during proton–electron combination, and

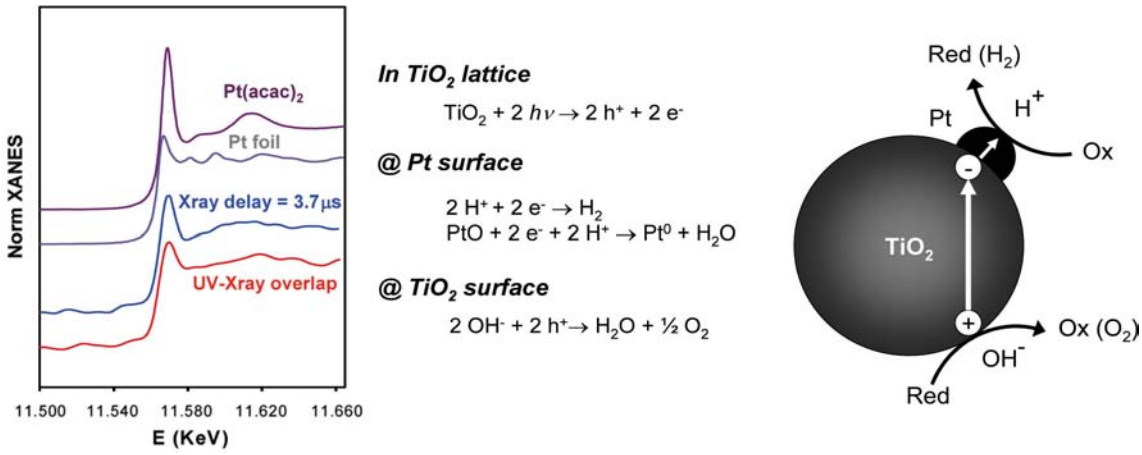

Figure 10
XANES of PtO/Pt on TiO_2 nanoparticle surface during the photoinduced redox reaction cycle compared with reference spectra of Pt(0) and Pt(II)acetoacetonate (AcAc).

(*c*) some Pt(0) was oxidized to Pt(II) in the water/methanol slurry after several microseconds of the photoexcitation (351 nm), possibly by the migration of oxygen formed on the surface of TiO_2 from the oxidation of the hydroxyl group. A detailed mechanism and interpretation require further investigation with a better signal-to-noise ratio of the data.

This example clearly indicates that the XTA measurements are sensitive to the transient oxidation state of the metal center when it undergoes the redox reaction. Because the MLCT states of metal complexes are normally the reactants for some water-splitting reactions, the identities of their excited state, their intermediate state after donating or accepting electrons and their final state at the end of the reaction cycle are all important to know in order to find a rational way of improving the reaction efficiency. XAS measurements with microsecond-to-millisecond time resolution have been carried out for some later catalytic reaction steps that are not directly induced by light, such as metal complex catalyzed water splitting as detected by time-resolved XAS studies on the Mn cluster of an oxygen evolving complex in photosystem II (Dau & Haumann, 2008, 2007; Grundmeier *et al.*, 2007)

5. Method development

The XTA methodology development at Argonne has been focused on enabling measurements of dilute samples ($\leq$1 m*M*), because many molecules have limited solubility and available quantities. The main challenge has been extracting maximum transient structural information from each X-ray photon under the pump–probe conditions which include temporal and spatial constraints as well as laser photon constraints, such as optical extinction coefficients, and available pump wavelengths. Reviews on the methodology of XTA have summarized the approaches in finding the optimal experimental conditions in this multi-dimensional space (Chen, 2005, 2004; Bressler & Chergui, 2004; Bressler *et al.*, 2008).

Our work until 2007 has been carried out at a wiggler beamline with X-ray fluorescence detection using a multi-element solid-state germanium detector array from Canberra (Jennings *et al.*, 2002). The advantage of such a detector is its capability of energy resolving desirable fluorescence signals from unwanted elastic scatterings and the low-pass filter fluorescence. The drawback of such a detector is its relatively long recovery time constant up to >1 μs limiting XTA experiments only during the single- or a few-bunch mode or a hybrid fill mode of the synchrotron operation. Since the beamline was upgraded to a dual in-line undulator beamline, the many-fold enhancement in photon flux overwhelmed the Canberra detector. Therefore, it is necessary to develop a new-generation detector system. So far, there has not been a commercially available detector system that simultaneously meets all the requirements for an ideal XTA experiment in dilute samples, such as multiple photon signal processing in one bunch, fast recovery time (<150 ns), energy resolution *etc*.

We have been using so far a detector system developed by Attenkofer and Jennings from the APS, which consists of a compact sample chamber integrating two photomultiplier tube or avalanche photodiode detectors, each coupled with plastic scintillator and a Soller-slits/elastic-scattering rejection filter set (Fig. 11). The detectors are operated in a current mode which allows the detection of multiple photon signals. In addition, the detector signals from the entire pulse train are digitized and processed using a noise-reduction algorithm, allowing signals from all X-ray pulses after the one synchronized with the pump laser pulses to be collected simultaneously in one measurement. The advantage of this detector system has been seen in XTA measurements for the RuN3/TiO_2 system which has multiple transient states corresponding to reaction rate constants on multiple time scales ranging from 10 fs to microseconds. Also, the enhanced signal quality in the second- and third-row transition metal complex data permits us to extract very small signal differences from where the structural parameters are extracted. The pitfall of such a simple detector system is the lack of energy-resolving power. When studying samples with more than two heavy elements,

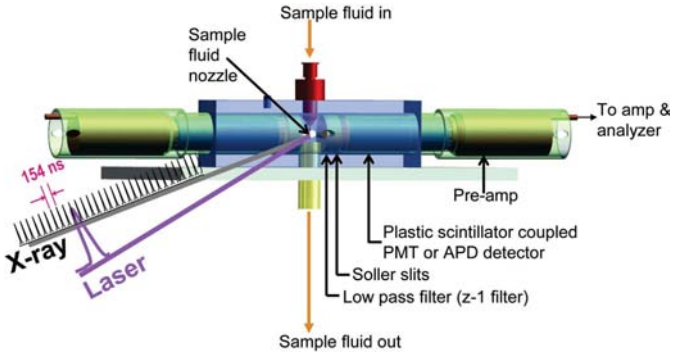

Figure 11
The new integrated sample/detector chamber unit used in XTA measurements.

the XAS spectrum for that with a higher-energy absorption edge is subject to interference with signals from that with a lower-energy absorption edge. The RuN3/TiO_2 system is one such example. Details of the detector system will be described in a future publication. Therefore, developing an ideal X-ray fluorescence detector is still under progress and needs significant effort in the community.

6. Summary and future studies

In the past decade, XTA has significantly impacted the understanding of fundamental chemical events and processes owing to its capability of obtaining transient molecular structural information during photochemical reactions. As this technique becomes more mature and more commonly used, some future developments are projected here with a focus on photochemistry.

Molecular systems. The advantages of XAS on probing local electronic and nuclear structures around a central X-ray absorbing atom in disordered media make the XTA technique well suited for probing metal centers whose excited-state structures, coordination geometries and oxidation states change during photochemical processes. These structural parameters are extremely important for understanding solar energy conversion in homogeneous and heterogeneous photocatalysis, photodriven molecular machines and enzymatic reactions. As the data acquisition becomes more effective, one can investigate biological metal center structures and irreversible photochemical processes with continuous unidirectional flow of liquid samples. It is conceivable that XTA in the new decade could approach a level of application like that of optical transient absorption for a broad range of systems far beyond the demonstration of the XTA feasibility.

Ultrafast X-ray capability. As X-ray pulses become as short as several femtoseconds, the coherent interference between the pump and probe pulses may have to be considered (Mukamel, 2000). In a longer time regime of a few picoseconds, structures of many equilibrated states with lifetimes much shorter than the current 100 ps time resolution from synchrotron sources can be obtained. These states can be exemplified by the first excited states of NiTPP and $[Cu(dmp)_2]^+$ with lifetimes in the picosecond range. Developing other spectroscopic techniques, such as resonant inelastic X-ray scattering (Glatzel & Bergmann, 2005; Shirley, 1998), will be one of the future developments in X-ray spectroscopy with femtosecond time resolution from X-ray free-electron laser facilities with monochromatic photons.

Combination of XAFS and wide-angle X-ray scattering (WAXS). Because XTA probes local structures surrounding a heavy atom, it is incapable of determining the overall shape of molecules in solution and salvation processes that take place at a distant part of the molecule from the metal center. X-ray transient scattering (XTS) in both small- and wide-angle ranges incorporating the laser pump pulse combined with XTA would enable us to obtain complete structural information on excited states or reaction intermediates in photochemical reactions. For photochemical processes with more complicated molecular systems, the local structures can be obtained by XTA, while the overall molecular size and shape as well as finer structures can be obtained by XTS. This has been demonstrated by a recent study on the structural determination for supramolecular assemblies with modular building blocks in solution by WAXS at a third-generation synchrotron source (Tiede *et al.*, 2004; Cammarata *et al.*, 2006; Kong *et al.*, 2008). A combination of LITR-XAS together with WAXS will greatly enhance the capability of structural determination during photochemical processes on different length scales.

Theoretical studies. Although high-precision transient molecular structures obtained from XTA are informative, one needs to reveal details on the energy levels of molecular orbitals and the excited-state electronic density distribution as well as nuclear coordinates from computational results. Hence, it is very desirable and important that both experimental and theoretical capabilities are developed synergistically. Currently, excited-state structural calculations, especially for metal complexes, are few and mostly carried out using the density functional theory (Furche & Ahlrichs, 2002). Because the X-ray pulse duration from current synchrotron sources is much longer than X-ray photon events, such as X-ray fluorescence, most of the time-resolved structural studies exclude interactions between laser photons and X-ray photons. As the femtosecond X-ray sources emerge, extensive theoretical calculations involving interplays between two types of excitation processes are needed (Mukamel, 2000). Meanwhile, in order to maximize the structural information obtained from each X-ray photon, accurate computations on the correspondence of experimental XAS spectra and dynamic molecular structures is necessary.

We believe that time-resolved X-ray structural techniques will grow into a more common structural technique for the needs of observing, correlating and controlling structure and functions of molecules in the next decade, realising our dream of seeing molecules in action and controlling the actions towards targeted products.

The experimental work was funded by the Division of Chemical Sciences, Geosciences and Biosciences, Office of

Basic Energy Sciences of the US Department of Energy through Grant DE-AC02-06CH11357 (LX, XZ, JVL, AB, KA and GJ). The authors would like to thank Drs Wighard Jäger, Tao Liu, George B. Shaw, Erik C. Wasinger, David J. Gosztola, Jan Hessler, Andrew Goshe and Grigory Smolentsev for their contributions to the XTA work. LXC is very grateful for the collaborations with Professors Gerald J. Meyer, Jonathan S. Lindsey, Michael D. Hopkins, Michael R. Wasielewski, F. Castellano, Alexander V. Soldatov and Danial G. Nocera and their groups in various institutions. The ongoing collaboration with Dr David M. Tiede and the Photosynthesis Group at Argonne is also gratefully acknowledged. The long-time support from the Sector 11 and 12 staff at the Advanced Photon Source has been invaluable to the work presented here. Use of the Advanced Photon Source was supported by the US Department of Energy, Office of Science, Office of Basic Energy Sciences, under Contract No. DE-AC02-06CH11357.

References

Anderson, N. & Lian, T. (2005). *Annu. Rev. Phys. Chem.* **56**, 491–519.

Armaroli, N. (2001). *Chem. Soc. Rev.* **30**, 113–124.

Armaroli, N. (2008). *Chem. Phys. Chem.* **9**, 371–373.

Bach, U., Lupo, D., Comte, P., Moser, J. E., Weissortel, F., Salbeck, J., Spreitzer, H. & Gratzel, M. (1998). *Nature (London)*, **395**, 583–585.

Ballhausen (1962). *Introduction to Ligand Field Theory.* New York: McGraw-Hill.

Benfatto, M. & Della Longa, S. (2001). *J. Synchrotron Rad.* **8**, 1087–1094.

Benfatto, M., Della Longa, S., Hatada, K., Hayakawa, K., Gawelda, W., Bressler, C. & Chergui, M. (2006). *J. Phys. Chem. B*, **110**, 14035–14039.

Benko, G., Kallioinen, J., Myllyperkio, P., Trif, F., Korppi-Tommola, J. E. I., Yartsev, A. P. & Sundstrom, V. (2004). *J. Phys. Chem. B*, **108**, 2862–2867.

Bixon, M., Jortner, J., Cortes, J., Heitele, H. & Michel-Beyerle, M. E. (1994). *J. Phys. Chem.* **98**, 7289–7299.

Blankenship, R. E. (2002). *Molecular Mechanisms of Photosynthesis.* Oxford: Balckwell Science.

Bocarsly, A. B., Cameron, R. E., Mayr, A. & McDermott, G. A. (1987). *Photochemistry and Photophysics of Tungsten Carbyne Complexes, Photochemistry and Photophysics of Coordination Compounds*, edited by H. Yersin and A. Vogler. Berlin: Springer-Verlag.

Bocarsly, A. B., Cameron, R. E., Rubin, H.-D., McDermott, G. A., Wolff, C. R. & Mayr, A. (1985). *Inorg. Chem.* **24**, 3976–3978.

Bressler, C., Abela, R. & Chergui, M. (2008). *Z. Kristallogr.* **223**, 307–321.

Bressler, C. & Chergui, M. (2004). *Chem. Rev.* **104**, 1781–1812.

Bressler, C., Milne, C., Pham, V. T., ElNahhas, A., van der Veen, R. M., Gawelda, W., Johnson, S., Beaud, P., Grolimund, D., Kaiser, M., Borca, C. N., Ingold, G., Abela, R. & Chergui, M. (2009). *Science*, **323**, 489–492.

Cammarata, M., Lorenc, M., Kim, T. K., Lee, J. H., Kong, Q. Y., Pontecorvo, E., Lo Russo, M., Schiro, G., Cupane, A., Wulff, M. & Ihee, H. (2006). *J. Chem. Phys.* **124**, 124504.

Cannizzo, A., van Mourik, F., Gawelda, W., Zgrablic, G., Bressler, C. & Chergui, M. (2006). *Angew. Chem. Intl. Ed.* **45**, 3174–3176.

Carter, J. D., Kingsbury, K. B., Wilde, A., Schoch, T. K., Leep, C. J., Pham, E. K. & McElweewhite, L. (1991). *J. Am. Chem. Soc.* **113**, 2947–2954.

Castellano, F. N. & Meyer, G. J. (1997). *Prog. Inorg. Chem.* **44**, 167–208.

Cavalheiro, C. C. S., Torraca, K. E., Schanze, K. S. & McElwee-White, L. (1999). *Inorg. Chem.* **38**, 3254.

Cavalleri, A., Rini, M., Chong, H. H. W., Fourmaux, S., Glover, T. E., Heimann, P. A., Kieffer, J. C. & Schoenlein, R. W. (2005). *Phys. Rev. Lett.* **95**, 067405.

Chen, L. X. (2001). *J. Electron. Spectrosc.* **119**, 161–174.

Chen, L. X. (2003). *Faraday Discuss.* **122**, 315–329.

Chen, L. X. (2004). *Angew. Chem. Intl. Ed.* **43**, 2886–2905.

Chen, L. X. (2005). *Ann. Rev. Phys. Chem.* **56**, 221–254.

Chen, L. X., Jager, W. J. H., Jennings, G., Gosztola, D. J., Munkholm, A. & Hessler, J. P. (2001). *Science*, **292**, 262–264.

Chen, L. X., Jennings, G., Liu, T., Gosztola, D. J., Hessler, J. P., Scaltrito, D. V. & Meyer, G. J. (2002). *J. Am. Chem. Soc.* **124**, 10861–10867.

Chen, L. X., Shaw, G. B., Liu, T., Jennings, G. & Attenkofer, K. (2004). *Chem. Phys.* **299**, 215–223.

Chen, L. X., Shaw, G. B., Novozhilova, I., Liu, T., Jennings, G., Attenkofer, K., Meyer, G. J. & Coppens, P. (2003*a*). *J. Am. Chem. Soc.* **125**, 7022–7034.

Chen, L. X., Shaw, G. B., Novozhilova, I., Liu, T., Jennings, G., Attenkofer, K., Meyer, G. J. & Coppens, P. (2003*b*). *J. Am. Chem. Soc.* **125**, 7022–7034.

Chen, L. X., Shaw, G. B., Wasinger, E. C., Zhang, X., Attenkofer, K. & Jennings, G. (2006). *13th International Conference on X-ray Absorption Fine Structure (XAFS-13)*, edited by B. Hedman and P. Painetta, pp. 844–848, Stanford, CA, USA.

Chen, L. X., Zhang, X., Wasinger, E. C., Attenkofer, K., Jennings, G., Muresan, A. & Lindsey Jonathan, S. (2007). *J. Am. Chem. Soc.* **129**, 9616–9618.

Chen, L. X., Zhang, X., Wasinger, E. C., Lockard, J. V., Attenkofer, K., Jennings, G., Smolentsev, G. & Soldatov, A. V. (2010). In preparation.

Cherepy, N. J., Smestad, G. P., Gratzel, M. & Zhang, J. Z. (1997). *J. Phys. Chem. B*, **101**, 9342–9351.

Collin, J.-P., Dietrich-Buchecker, C., Gavina, P., Jimenez-Molero, M. C. & Sauvage, J.-P. (2001). *Acc. Chem. Res.* **34**, 477–487.

Collman, J. P., Marrocco, M., Denisevich, P., Koval, C. & Anson, F. C. (1979). *J. Electroanal. Chem.* **101**, 117–122.

Cunningham, K. L., McNett, K. M., Pierce, R. A., Davis, K. A., Harris, H. H., Falck, D. M. & McMillin, D. R. (1997). *Inorg. Chem.* **36**, 608–613.

Dau, H. & Haumann, M. (2007). *Photosyn. Res.* **92**, 327–343.

Dau, H. & Haumann, M. (2008). *Coord. Chem. Rev.* **252**, 273–295.

Della-Longa, S., Chen, L. X., Frank, P., Hayakawa, K., Hatada, K. & Benfatto, M. (2009). *Inorg. Chem.* **48**, 3934–3942.

Eom, H. S., Jeoung, S. C., Kim, D., Ha, J.-H. & Kim, Y.-R. (1997). *J. Phys. Chem. A*, **101**, 3661–3669.

Esswein, M. J. & Nocera, D. G. (2007). *Chem. Rev.* **107**, 4022–4047.

Freed, K. F. & Jortner, J. (1970). *J. Chem. Phys.* **52**, 6272–6291.

Fujishima, A. & Honda, K. (1972). *Nature (London)*, **238**, 37–39.

Furche, F. & Ahlrichs, R. (2002). *J. Chem. Phys.* **117**, 7433–7447.

Gawelda, W., Cannizzo, A., Pham, V. T., van Mourik, F., Bressler, C. & Chergui, M. (2007*a*). *J. Am. Chem. Soc.* **129**, 8199–8206.

Gawelda, W., Pham, V. T., Benfatto, M., Zaushitsyn, Y., Kaiser, M., Grolimund, D., Johnson, S. L., Abela, R., Hauser, A., Bressler, C. & Chergui, M. (2007*b*). *Phys. Rev. Lett.* **98**, 057401.

Gentemann, S., Nelson, N. Y., Jaquinod, L., Nurco, D. J., Leung, S. H., Medforth, C. J., Smith, K. M., Fajer, J. & Holten, D. (1997). *J. Phys. Chem. B*, **101**, 1247–1254.

Glatzel, P. & Bergmann, U. (2005). *Coord. Chem. Rev.* **249**, 65–95.

Gratzel, M. (2001). *Nature (London)*, **414**, 338–344.

Grundmeier, A., Loja, P., Haumann, M. & Dau, H. (2007). *Photosyn. Res.* **91**, PS446.

Hamalainen, R., Algren, M., Turpeinen, U. & Raikas, T. (1979). *Crystal Structure Commun.* **8**, 75–80. http://www.lightsources.org/cms/.

Iwamura, M., Takeuchi, S. & Tahara, T. (2007). *J. Am. Chem. Soc.* **129**, 5248–5256.

Jelliss, P. A. & Wampler, K. M. (2005). *Organometallics*, **24**, 707–714.
Jennings, G., Jaeger, W. J. H. & Chen, L. X. (2002). *Rev. Sci. Instrum.* **72**, 362–368.
Jia, S.-L., Jentzen, W., Shang, M., Song, X.-Z., Ma, J.-G., Scheidt, W. R. & Shelnutt, J. A. (1998). *Inorg. Chem.* **37**, 4402–4412.
Kalyanasundaram, K. (1992). *Photochemistry of Polypyridine and Porphyrin Complexes.* London: Academic Press.
Kau, L.-S., Spira-Solomon, D. J., Penner-Hahn, J. E., Hodgson, K. O. & Solomon, E. I. (1987). *J. Am. Chem. Soc.* **109**, 6433–6442.
Khalil, M., Marcus, M. A., Smeigh, A. L., McCusker, J. K., Chong, H. H. W. & Schoenlein, R. W. (2006). *15th International Conference on Ultrafast Phenomena*, edited by P. Corkum, D. Jonas, R. J. D. Miller and A. M. Weiner, pp. 722–724. Pacific Grove, CA, USA.
Kim, D. & Holten, D. (1983). *Chem. Phys. Lett.* **98**, 584–589.
Kim, D., Holten, D. & Gouterman, M. (1984). *J. Am. Chem. Soc.* **106**, 2793–2798.
Kim, D., Kirmaier, C. & Holten, D. (1983). *Chem. Phys.* **75**, 305–322.
Kong, Q. Y., Lee, J. H., Plech, A., Wulff, M., Ihee, H. & Koch, M. H. J. (2008). *Angew. Chem. Intl Ed.* **47**, 5550–5553.
Kruglik, S. G., Apanasevich, P. A., Chirvony, V. S., Kvach, V. V. & Orlovich, V. A. (1995). *J. Phys. Chem.* **99**, 2978–2995.
Lai, S.-W., Chan, M. C. W., Wang, Y., Lam, H.-W., Peng, S.-M. & Che, C. M. (2001). *J. Organomet. Chem.* **617–618**, 133.
Lamansky, S., Djurovich, P., Murphy, D., Abdel-Razzaq, F., Lee, H. E., Adachi, C., Burrows, P. E., Forrest, S. R. & Thompson, M. E. (2001). *J. Am. Chem. Soc.* **123**, 4304–4312.
Lee, F. W., Chan, M. C. W., Cheung, K. K. & Che, C. M. (1998). *J. Organomet. Chem.* **552**, 255–263.
Lemke, C., Dreybrodt, W., Shelnutt, J. A., Quirke, J. M. E. & Schweitzer-Stenner, R. (1998). *J. Raman Spectrosc.* **29**, 945–953.
Lessing, J., Li, X., Lee, T. & Rose-Petruck, C. G. (2008). *J. Phys. Chem. A*, **112**, 2282–2292.
Lind, S. J., Gordon, K. C. & Waterland, M. R. (2008). *J. Raman Spectrosc.* **39**, 1556–1567.
Liu, F., Cunningham, K. L., Uphues, W., Fink, G. W., Schmolt, J. & McMillin, D. R. (1995). *Inorg. Chem.* **34**, 2015–2018.
Lockard, J. V., Stickrath, A. B., Zhang, X., Atenkoffer, K., Smolentsev, G., Rachford, A., Wang, X., Castellano, F. N., Soldatov, A. V. & Chen, L. X. (2010). In preparation.
Lovaasen, B. M., Lockard, J. V., Stickrath, A. B., Chen, L. X. & Hopkins, M. D. (2010). In preparation.
Lu, W., Mi, B. X., Chan, M. C. W., Hui, Z., Che, C. M., Zhu, N. Y. & Lee, S. T. (2004). *J. Am. Chem. Soc.* **126**, 4958–4971.
Lyon, D. K., Miller, W. K., Novet, T., Domaille, P. J., Evitt, E., Johnson, D. C. & Finke, R. G. (1991). *J. Am. Chem. Soc.* **113**, 7209–7221.
McMillin, D. R., Hudson, B. P., Liu, F., Sou, J., Berger, D. J. & Meadows, K. A. (1993). *Adv. Chem. Ser.* **238**, 211–231.
McMillin, D. R., Kirchhoff, J. R. & Goodwin, K. V. (1985). *Coord. Chem. Rev.* **64**, 83–92.
McMillin, D. R., Liu, F., Meadows, K. A., Aldridge, T. K. & Hudson, B. P. (1994). *Coord. Chem. Rev.* **132**, 105–112.
McMillin, D. R. & McNett, K. M. (1998). *Chem. Rev.* **98**, 1201–1219.
Mayr, A., Yu, M. P. Y. & Yam, V. W. W. (1999). *J. Am. Chem. Soc.* **121**, 1760–1761.
Miller, M. T., Gantzel, P. K. & Karpishin, T. B. (1999). *J. Am. Chem. Soc.* **121**, 4292–4293.
Mukamel, S. (2000). *Annu. Rev. Phys. Chem.* **51**, 691–729.
Nam, W. O., Lim, M. H., Lee, H. J. & Kim, C. (2000). *J. Am. Chem. Soc.* **122**, 6641–6647.
Nozawa, S. *et al.* (2007). *J. Synchrotron Rad.* **14**, 313–319.
Oertling, W. A., Salehi, A., Chung, Y. C., Leroi, G. E., Chang, C. K. & Babcock, G. T. (1987). *J. Phys. Chem.* **91**, 5887–5898.
Oulianov, D. A., Tornov, I. V., Dvornikov, A. S. & Rentzepis, P. M. (2002). *Proc. Natl Acad. Sci. USA*, **99**, 12556–12561.
Pollagi, T. P., Geib, S. J. & Hopkins, M. D. (1994). *J. Am. Chem. Soc.* **116**, 6051–6052.
Rodriguez, J. & Holten, D. (1989). *J. Chem. Phys.* **91**, 3525–3531.
Rodriguez, J. & Holten, D. (1990). *J. Chem. Phys.* **92**, 5944–5950.
Rosenthal, J. & Nocera, D. G. (2007). *Oxygen Activation Chemistry of Pacman and Hangman Porphyrin Architectures Based on Xanthene and Dibenzofuran Spacers*, Vol. **55**, pp. 483–544.
Ruthkosky, M., Kelly, C. A., Zaros, M. C. & Meyer, G. J. (1997). *J. Am. Chem. Soc.* **119**, 12004–12005.
Saes, M., Bressler, C., Abela, R., Grolimund, D., Johnson, S. L., Heimann, P. A. & Chergui, M. (2003). *Phys. Rev. Lett.* **90**, 047403.
Sauvage, J.-P. (1998). *Acc. Chem. Res.* **31**, 611–619.
Sauvage, J.-P. (2001). *Science*, **291**, 2105–2106.
Scaltrito, D. V., Kelly, C. A., Ruthkosky, M., Zaros, M. C. & Meyer, G. J. (2000*a*). *Inorg. Chem.* **39**, 3765–3770.
Scaltrito, D. V., Thompson, D. W., O'Callaghan, J. A. & Meyer, G. J. (2000*b*). *Coord. Chem. Rev.* **208**, 243–266.
Schoch, T. K., Main, A. D., Burton, R. D., Lucia, L. A., Robinson, E. A., Schanze, K. S. & McElweeWhite, L. (1996). *Inorg. Chem.* **35**, 7769–7775.
Schweitzer-Stenner, R., Lemke, C., Haddad, R., Qiu, Y., Shelnutt, J. A., Quirke, J. M. E. & Dreybrodt, W. (2001). *J. Phys. Chem. A*, **105**, 6680–6694.
Shan, F., Porter, R., Cheng, N., Masiel, D. J. & Guo, T. (2007). *J. Phys. Chem. C*, **111**, 4643–4647.
Shaw, G. B., Grant, C. D., Castner, E. W., Meyer, G. J. & Chen, L. X. (2007*a*). *J. Am. Chem. Soc.* **129**, 2147–2160.
Shaw, G. B., Grant, C. D., Shirota, H., Castner, E. W., Meyer, G. J. & Chen, L. X. (2007*b*). *J. Am. Chem. Soc.* **129**, 2147–2160.
Shelnutt, J. A., Straub, K. D., Rentzenpis, P. M. & Gouterman, M. (1984). *Biochemistry*, **23**, 3946.
Shirley, E. L. (1998). *Phys. Rev. Lett.* **80**, 794–797.
Shvedko, A. G., Kruglik, S. G., Ermolenkov, V. V., Orlovich, V. A., Turpin, P. Y., Greve, J. & Otto, C. (1999). *J. Raman Spectrosc.* **30**, 677–684.
Siddique, Z. A., Yamamoto, Y., Ohno, T. & Nozaki, K. (2003). *Inorg. Chem.* **42**, 6366–6378.
Simpson, C. K., Da Re, R. E., Pollagi, T. P., Steele, I. M., Dallinger, R. F. & Hopkins, M. D. (2003). *Inorg. Chim. Acta*, **345**, 309–319.
Smeigh, A. L. & McCusker, J. K. (2006). *15th International Conference on Ultrafast Phenomena*, edited by P. Corkum, D. Jonas, R. J. D. Miller and A. M. Weiner, pp. 273–275. Pacific Grove, CA, USA.
Smith, T. A., Penner-Hahn, J. E., Berding, M. A., Doniach, S. & Hodgson, K. O. (1985). *J. Am. Chem. Soc.* **107**, 5945–5955.
Smolentsev, G. & Soldatov, A. (2006). *J. Synchrotron Rad.* **13**, 19–29.
Smolentsev, G. & Soldatov, A. V. (2007). *Comput. Mater. Sci.* **39**, 569–574.
Smolentsev, G., Soldatov, A. V. & Chen, L. X. (2008). *J. Phys. Chem. A*, **112**, 5363–5367.
The Porphyrin Handbook (1999). New York: Academic Press.
Tiede, D. M., Zhang, R. T., Chen, L. X., Yu, L. H. & Lindsey, J. S. (2004). *J. Am. Chem. Soc.* **126**, 14054–14062.
Trammell, S., Sullivan, B. P., Hodges, L. M., Harman, W. D., Smith, S. R. & Thorp, H. H. (1995). *Inorg. Chem.* **34**, 2791–2792.
Van der Poel, W. A. J. A., Nuijs, A. M., Noort, M. & Van der Waals, J. H. (1982). *J. Phys. Chem.* **86**, 5191–5197.
Veen, R. M. van der, Milne, C. J., El Nahhas, A., Lima, F. A., Pham, V. T., Best, J., Weinstein, J. A., Borca, C. N., Abela, R., Bressler, C. & Chergui, M. (2009). *Angew. Chem. Intl Ed.* **48**, 2711–2714.
Xue, W. M., Chan, M. C. W., Mak, T. C. W. & Che, C. M. (1997). *Inorg. Chem.* **36**, 6437–6439.
Xue, W. M., Wang, Y., Chan, M. C. W., Su, Z. M., Cheung, K. K. & Che, C. M. (1998). *Organometallics*, **17**, 1946.
Xue, W. M., Wang, Y., Mak, T. C. W. & Che, C. M. (1996). *J. Chem. Soc. Dalton Trans.* pp. 2827–2834.
Zhang, X., Lockard, J. V., Guo, J., Attenkofer, K., Jennings, G. & Chen, L. X. (2010). In preparation.
Zhang, X. Y., Wasinger, E. C., Muresan, A. Z., Attenkofer, K., Jennings, G., Lindsey, J. S. & Chen, L. X. (2007). *J. Phys. Chem. A*, **111**, 11736–11742.